Article

Synthesis and Characterization of Magnetite/Gold Core Shell Nanoparticles Stabilized with a β-Cyclodextrin Nanosponge to Develop a Magneto-Plasmonic System

Sebastián Salazar Sandoval [1,2,3,4,*] , Daniel Santibáñez [1], Ana Riveros [2,3], Fabián Araneda [5], Tamara Bruna [6], Nataly Silva [4], Nicolás Yutronic [1], Marcelo J. Kogan [2,3] and Paul Jara [1,*]

1 Departamento de Química, Facultad de Ciencias, Universidad de Chile, Las Palmeras 3425, Ñuñoa 7610658, Chile; daniel.santibanez@ug.uchile.cl (D.S.); nyutroni@uchile.cl (N.Y.)
2 Departamento de Química Farmacológica y Toxicológica, Universidad de Chile, Sergio Livingstone 1007, Santiago 8380492, Chile; riveros.ana@gmail.com (A.R.); mkogan@ciq.uchile.cl (M.J.K.)
3 Advanced Center for Chronic Diseases (ACCDiS), Universidad de Chile, Santos Dumont 964, Independencia 8380494, Chile
4 Facultad de Diseño, Universidad del Desarrollo, Avenida Plaza 680, Las Condes 7610658, Chile; nrsilva@udd.cl
5 Departamento de Física, Center for the Development of Nanoscience and Nanotechnology (CEDENNA), Universidad de Santiago de Chile, Santiago 9170022, Chile; naibaf.araneda@gmail.com
6 Centro de Investigación Austral Biotech, Facultad de Ciencias, Universidad Santo Tomás, Avenida Ejército 146, Santiago 8320000, Chile; tbruna@santotomas.cl
* Correspondence: sebasalazar@ug.uchile.cl (S.S.S.); pjara@uchile.cl (P.J.); Tel.: +56-229787396 (P.J.)

Abstract: Magnetite/gold core-shell nanoparticles (magnetite/gold NPs) have important optical and magnetic properties that provide potential for applications, especially biomedical ones. However, their preparation is not exempt from difficulties that might lead to unexpected or undesired structures. This work reports the synthesis and characterization of magnetite/gold NPs using tetramethylammonium hydroxide (TMAH) to promote the formation of a continuous interface between the magnetite core and the thin gold shell. The synthesized magnetite/gold NPs were characterized using transmission electron microscopy (TEM), energy-dispersive spectroscopy (EDS), field emission scanning electron microscope (FE-SEM), ζ-potential, vibrating sample magnetometer (VSM), selected area electron diffraction (SAED), UV-Visible spectroscopy, and dynamic light scattering (DLS), confirming the core-shell structure of the NPs with narrow size distribution while evidencing its plasmonic and superparamagnetic properties as well. Further, the magnetite/gold NPs were associated and stabilized with a β-cyclodextrin nanosponge (β-CDNSs), obtaining a versatile magneto-plasmonic system for potential applications in the encapsulation and controlled release of drugs.

Keywords: gold-magnetite nanoparticles; core-shell nanoparticles; superparamagnetic nanoparticles; surface plasmon resonance; magneto-plasmonic nanoparticles; cyclodextrin polymers

1. Introduction

Magnetite/gold core-shell NPs have unique magneto-plasmonic properties. These NPs are used in biomedical applications, such as magnetic resonance imaging (MRI), photothermal therapy, controlled drug delivery, protein isolation, biosensing, and DNA detection [1–3]. Their physicochemical characteristics are also of interest to developing cancer therapy strategies, such as binding to drugs and ligands for tumor cell destruction and targeted drug delivery [4,5]. Magnetite NPs have been receiving notorious attention on their part due to their superparamagnetic properties and their potential applications in the fields of medicine and pharmaceutics [6,7]. Another nanomaterial that has been thoroughly studied is gold nanoparticles (AuNPs), known for exhibiting a resonant oscillating surface plasmon when exposed to the frequency of visible light. Thus, AuNPs have a vast

range of applications, which include electronics, photodynamic therapy, sensors, and drug delivery [8,9]. That said, gold and magnetite NPs have exciting properties that make them desirable to be combined on a single nanomaterial or nanocomposite.

Nevertheless, gold and magnetite NPs also have a fair number of shortcomings. For instance, AuNPs are short-lived in the bloodstream, and only a tiny amount binds to the organ or tissues when used for imaging [10]. Moreover, photothermal is limited to tissues close to the skin, and IR light only penetrates through thin tissues, not reaching deep inside [11,12]. On the other hand, magnetite NPs cannot bind to many macromolecules and have poor colloidal stability in physiological conditions, making their coating with a polymer or organic compound imperative [13,14].

To overcome such drawbacks, gold and magnetite NPs have been synthesized on a single nanomaterial. Magnetite/gold core-shell NPs have many advantages due to their low toxicity, plasmonic, and superparamagnetic nature [15,16]. Although various magneto-plasmonic NPs ranging in their morphology, size, and shape have been reported, such as gold and silver shells with a magnetite core [17], magnetite-gold nanoshells [18], dumbbell magnetite/gold NPs [19], and core-satellite magnetite/gold NPs [20], the most prominent core-shell shape consists in a concentric spherical one, which allows altering the core nanoparticle surface with another material, without compromising their properties. However, the synthetic routes present some disadvantages, promoting the formation of a magnetite-Au NPs composite rather than a core-shell structure [21].

In that regard, the surfactant molecules at the magnetite-gold interface might be essential in forming core-shell NPs. The use of tetramethylammonium hydroxide (TMAH) has been reported as a surfactant to facilitate the transition from an amorphous material to a crystalline phase, generating appropriate conditions for forming an enveloping layer of the noble metal [22]. That said, the colloidal stability of the magnetite/gold core-shell NPs is still an issue at hand.

β-cyclodextrins (β-CDs) are cyclic oligosaccharides widely used in pharmaceutical and medical formulations [23,24]. The cross-linking of β-CDs, using an appropriate organic linker, leads to the formation of a β-CD nanosponge (βCDNSs), which can be described as polymers with a plethora of lipophilic and hydrophilic interstices, suitable for the inclusion of a broad spectrum of drugs [25–29]. β-CDNSs have also been studied to stabilize noble metal nanoparticles, such as AuNPs [30–32], gold nanorods (AuNRs) [33], or silver nanoparticles (AgNPs) [34–36].

This work describes a method for synthesizing magnetite/gold core-shell systems and their further stabilization with βCDNSs. Figure 1 shows the schematic representation of the proposed binary system.
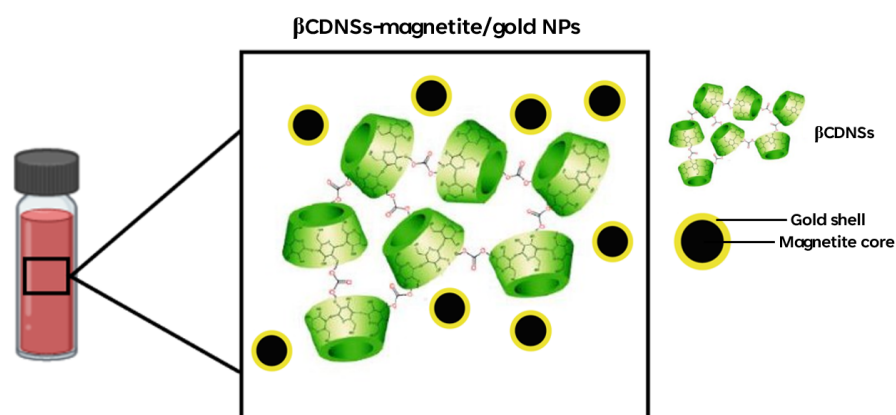
βCDNSs-magnetite/gold NPs

Figure 1. Schematic representation of βCDNSs association with magnetite/gold NPs.

In summary, this article shows experimental evidence for forming a continuous interface between the surface of a magnetite core and the thin gold layer. The magnetite/gold

NPs were further deposited and stabilized on βCDNSs to obtain a magneto-plasmonic system with potential applications in drug delivery or encapsulation of therapeutic agents.

2. Materials and Methods

2.1. Materials

All reagents used for the synthesis of the nanomaterials were of analytical grade: β-cyclodextrin, $C_{42}H_{70}O_{35}$, 97%, 1134.9 g/mol; diphenyl carbonate, $C_{13}H_{10}O$, 99%, 214.2 g/mol; iron (III) chloride, $FeCl_3$, 97%, 162.2 g/mol; iron (II) chloride, $FeCl_2$, 97%, 126.7 g/mol; sodium hydroxide, NaOH, ≥99.9%, 39.9 g/mol; tetramethylammonium hydroxide, $(CH_3)_4N(OH)$, 25% wt. in H_2O, 91.1 g/mol; tetra chloroauric acid, $HAuCl_4$, ≥99.9%, 339.7 g/mol; sodium citrate tribasic dihydrate, $HOC(COONa)(CH_2COONa)_2 \cdot 2H_2O$, ≥99.9%, 294.1 g/mol, and purchased from Sigma-Aldrich (Darmstadt, Germany). Milli-Q water was obtained through a Millipore Direct 5 system. All glass material used for this work was extensively washed with aqua regia.

2.2. Synthesis of Magnetite Nanoparticles

Magnetite NPs were synthesized using a previously reported co-precipitation method [37,38] with slight modifications. $FeCl_2$ (0.1 M, 1 mL) and $FeCl_3$ (0.2 M, 4 mL) were prepared in 0.1 M HCl under an Ar gas supply to provide an inert atmosphere. The co-precipitation was performed by dropwise adding NaOH (1 M, 50 mL) under constant stirring. The reaction was kept until a black ferrofluid was formed. Finally, 1 mL of tetramethylammonium hydroxide (TMAH, 25% wt.) was added to the synthesized magnetite NPs. The magnetite NPs were separated using a neodymium alloy magnet (5000 G), washed with double-distilled water, and stored at 4 °C to prevent their oxidation to maghemite.

2.3. Synthesis of Magnetite-Gold Core-Shell Nanoparticles

The thin gold shell was synthesized in situ to obtain magnetite/gold NPs, as reported by previous procedures [2,39]. 1 mL of a 0.5% *v/v* $HAuCl_4$ solution was added to 30 mg of TMAH coated-magnetite NPs, suspended in 40 mL of Milli-Q water, and under reflux conditions (110 °C). After 10 min, 4 mL of a freshly prepared sodium citrate solution (1% wt.) was quickly added while stirring until the solution turned brownish-red. The developed magnetite/gold NPs were allowed to settle and cool to room temperature. The magnetic response of the obtained magnetite/gold NPs was evaluated using a neodymium magnet (5000 G), as illustrated in Figure A1 (see Appendix A).

2.4. Synthesis of the β-Cyclodextrin Polymer (βCDNSs)

βCDNSs were synthesized according to the melting method procedure [40]. The protocol was slightly modified to reduce the number of by-products, trace precursors and to increase yield. β-CD and diphenyl carbonate (DPC) were grounded and homogenized in a 1:4 molar ratio (1.5 g:0.85 g). Then, the solid mixture was heated to 100 °C for 5 h, under constant stirring. Afterward, the solid was left to cool at room temperature, washed with double distilled water and acetone through Soxhlet extraction, and dried at 80 °C for 24 h. The obtained βCDNSs were stored in a desiccator for further use.

2.5. Association of Magnetite/Gold Nanoparticles with βCDNSs

The βCDNSs were associated with the magnetite/gold NPs by adding 50 mg of the cyclodextrin polymer into 800 µL of magnetite/gold NPs. After settling for 15 min, the systems were centrifuged for 20 min. The βCDNSs turned from white to dark red upon deposition of magnetite/gold NPs. The obtained βCDNSs-magnetite/gold system was separated from the supernatant, washed with Milli-Q water, and resuspended to eliminate the uncomplexed magnetite/gold NPs.

2.6. Characterization of Magnetite, Magnetite/Gold, and βCDNSs-Magnetite/Gold NPs

TEM micrographs of magnetite, magnetite/gold, and βCDNSs-magnetite/gold NPs were obtained using a Tecnai ST F20, 200–800 kV HR-TEM instrument, operating at 120 kV and equipped with SAED and EDS. The samples were dispersed in an ethanolic solution (30% *v/v*), sonicated for 10 min, and deposited (5 μL) on a copper grid with a film of Formvar.

The surface morphology of βCDNSs-magnetite/gold NPs was analyzed through scanning electron microscopy (SEM) using a Zeiss LEO-Supra 35-VP with an acceleration voltage of 20 kV and equipped with an EDS. For measurements, the βCDNSs-magnetite/gold sample was dried and mounted on a metal stub with a carbon film.

The structure and morphology of the magnetite/gold NPs were elucidated using FE-SEM microscopy in an INSPECT-F50 FEI equipped with an EDS detector. The sample was prepared according to the procedure described for TEM analysis and deposited on a copper grid with a holey carbon film.

The hydrodynamic diameters (D_h), polydispersity indexes (PDI), and ζ-potentials for magnetite, Au-magnetite, and βCDNSs-magnetite/gold NPs were calculated using DLS Zetasizer NanoS series, Malvern. The samples were diluted using double-distilled water before measuring at 298 K, using the cumulant method to obtain the D_h and PDI values and the Smoluchowski approximation for the ζ-potentials.

UV-Visible spectrophotometry was performed to ascertain the presence of the surface plasmon resonance in the magnetite/gold and βCDNSs-magnetite/gold NPs. The spectra were obtained using a Perkin Elmer, Lambda 25 UV-Visible spectrometer and processed with the UVProve 1.10 software. The measurements were conducted in a 200–700 nm range, with deionized water as a reference.

The saturation magnetization of magnetite, magnetite/gold, and βCDNSs-magnetite/gold NPs was determined using a homemade vibrating sample magnetometer (VSM). The hysteresis curves were obtained with the following parameters: 50 mg of each sample, a magnetic field range from −8000 to 8000 Oersted, and 298 K.

Fourier transform infrared (FT-IR) spectra of βCDNSs, and βCDNS-magnetite/gold NPs were obtained using a Jasco FT-IR 4600 spectrometer. One hundred fifty scans per sample were performed at 298 K in a 400–4000 cm^{-1} range. CO_2, H_2O, and KBr baseline correction were made with the Spectra Manager Software (Jasco, PA, USA).

Determination of Fe and Au content in the magnetite/gold and βCDNSs-magnetite/gold NPs was performed through atomic absorption spectrophotometry (AAS) using a Perkin-Elmer Model 5100. The samples were dried at 60 °C, digested in 1 M HNO_3 and 1 M HCl (1 mL each), and diluted suitably (1:2 *v/v*) before measurements at 1800 °C and in air-acetylene flame. Gold (1000 mg Au; $HAuCl_4$ in 12.7% HCl) and iron (1000 mg Fe; $FeCl_3$ in 15% HCl) standards (Sigma-Aldrich, Saint Louis, MO, USA) were used for the calibration curves.

3. Results and Discussion

3.1. Characterization of the Synthesized Magnetite/Gold NPs

The morphology and mean size of the synthesized magnetite/gold NPs were elucidated through TEM and HR-TEM analyses. Figure 2 illustrates the TEM micrographs of bare magnetite (A) and magnetite/gold NPs (B), whereas Figure 2C,D depicts the images of magnetite/gold NPs obtained with HR-TEM. Bare magnetite NPs were found to be 15 ± 3 nm with spherical morphology. TEM images of magnetite/gold NPs allowed us to identify a thin coating surrounding the magnetite core, with a shell thickness of roughly ~2 ± 0.1 nm, while retaining the spherical morphology of bare magnetite and a mean size of 20 ± 5 nm.

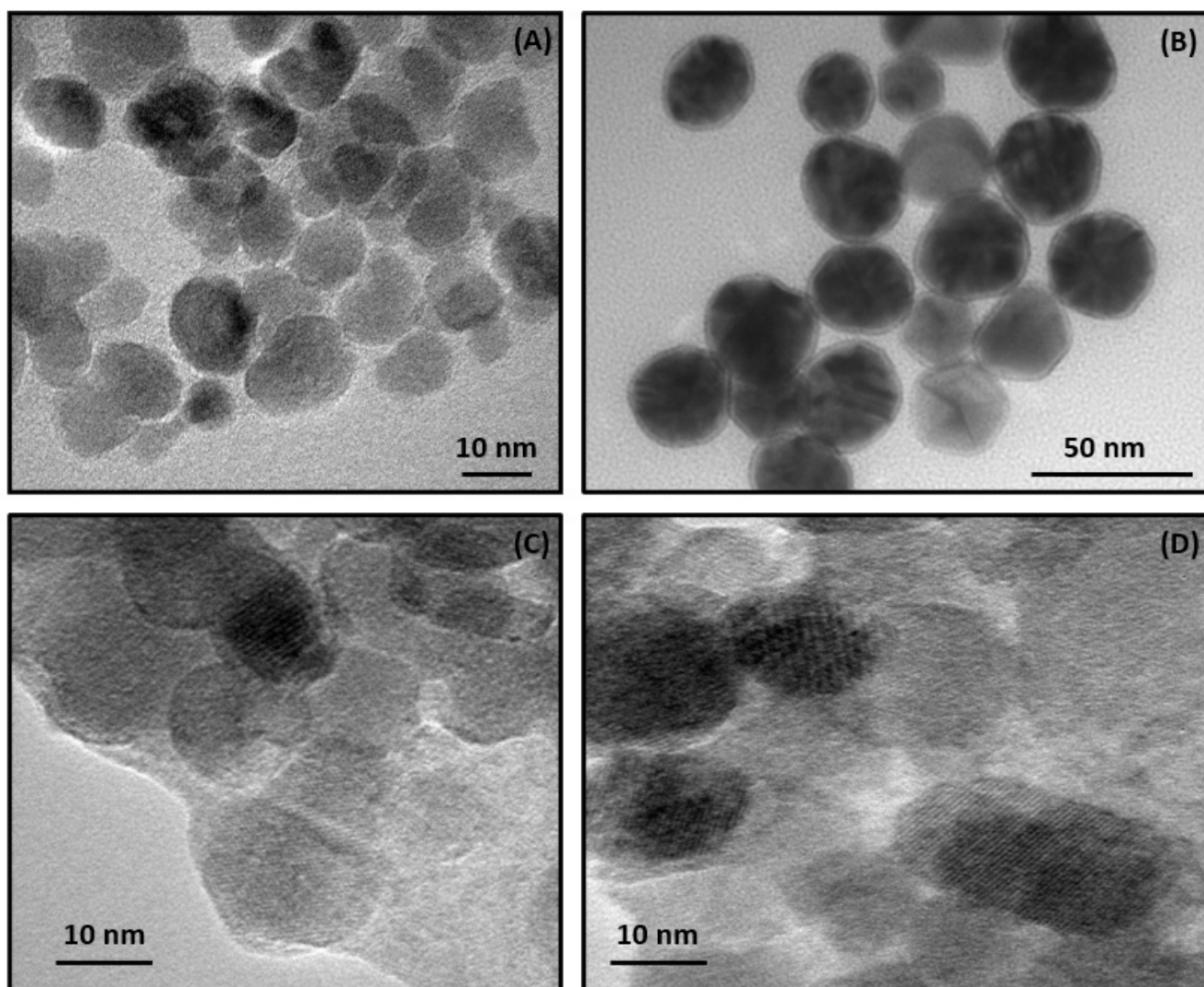**Figure 2.** TEM micrographs of bare magnetite (**A**) and magnetite/gold NPs (**B**); HR-TEM (**C**,**D**) micrographs of the synthesized magnetite/gold NPs.

HR-TEM was performed to confirm these findings, exhibiting that the most prominent interstitial lattice plane that can be indexed to the crystalline structure of magnetite (0.25 nm, 311) [41–43]. While uncoated magnetite NPs were still observed in the micrographs, it is possible to ascertain that a core-shell interface has formed (for further information on the size distribution measured from TEM, see Appendix A).

TMAH plays an essential role as a capping agent, required for the reduced gold to coat the surface of magnetite NPs, as it can be replaced through ligand exchange with another capping agent, such as sodium citrate [44,45]. The absence of capping agents might lead to a mixture of coated and uncoated particles or the formation of AuNPs separately, as the magnetite NPs surface is unavailable as a nucleation site. The obtained magnetite-gold system without using TMAH as a capping agent was characterized by TEM micrographs, which are summarized in Figure 3.

To corroborate the presence of Au in the thin layer, the SAED of magnetite/gold NPs was performed and compared to that of bare magnetite, as shown in Figure 4. Bare magnetite NPs (Figure 4A–C) evidenced diffraction patterns of 0.298, 0.256, 0.211, 0.173, 0.163, and 0.148 nm, which are consistent with magnetite (220), (311), (400), (422), (511), and (440) crystalline arrays of spacing, respectively (adapted from reference [46]). The analysis of magnetite/gold NPs (Figure 4B–D) exhibited the interstitial planes of bare magnetite, with new lattice fringes of 0.237 and 0.205 nm, which correspond to the (111) and (200)

crystalline structure of Au [47]. Moreover, EDS was performed to confirm the presence of both Fe and Au in the developed core-shell structure (see Figure 5). The detection of C and Cu is attributed to the composition of the grid. The distribution of Au within the Fe core was also investigated using elemental EDS mapping, as illustrated in Figure 5. The analysis demonstrated that the location of Au and Fe in the sample is strongly correlated, revealing a homogeneous distribution of Au all over the magnetite NPs, with a Fe/Au atomic ratio of 7.1, consistent with the dominant signals provided by the Fe core.
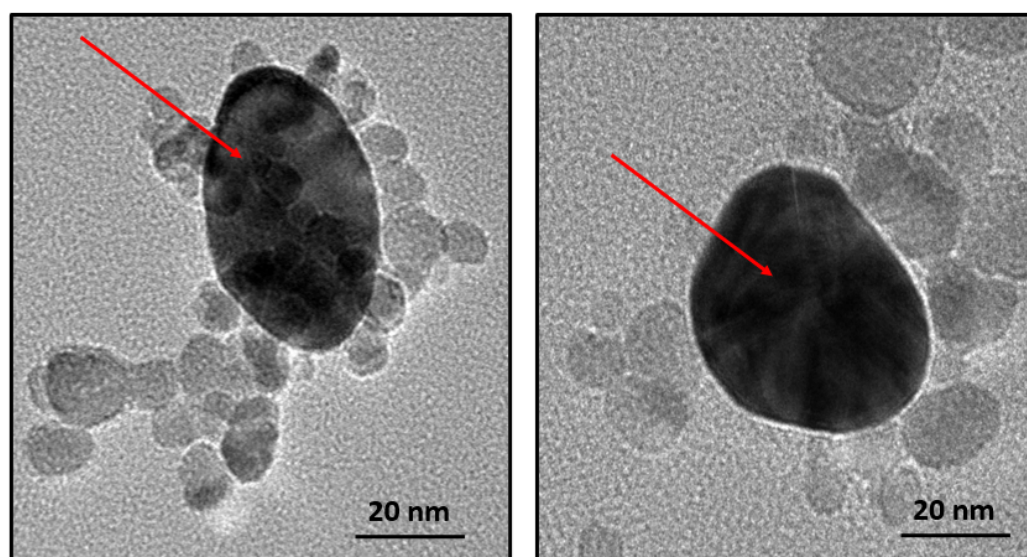

Figure 3. TEM micrographs of magnetite/gold NPs without using TMAH as a capping agent. AuNPs (highlighted with red arrows) are formed separately rather than in a core-shell structure.
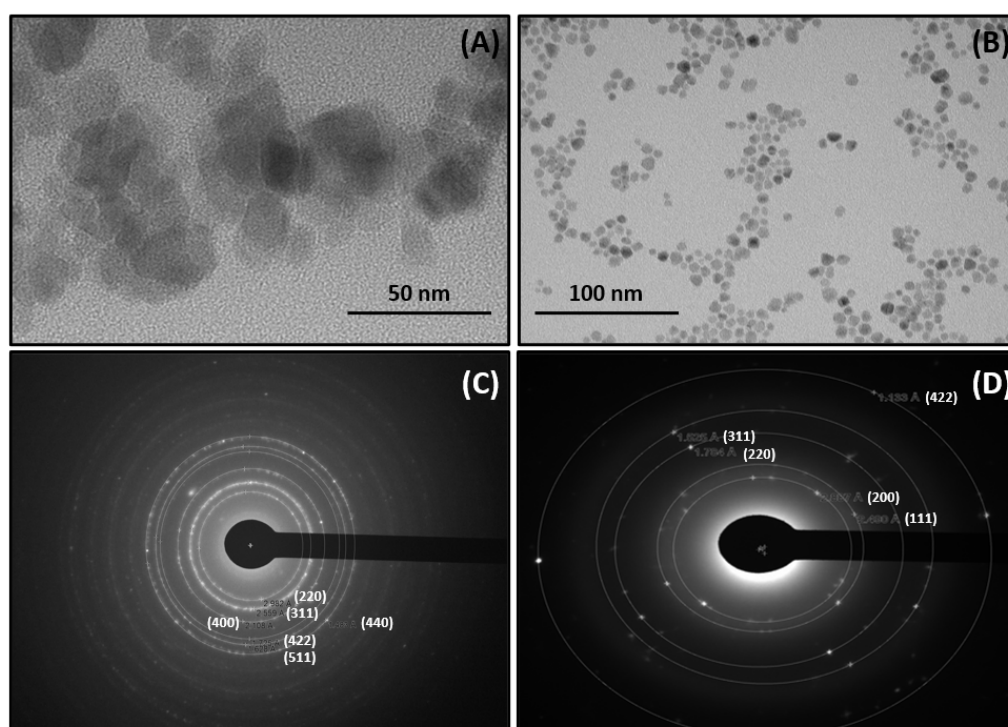

Figure 4. Selected areas and SAED patterns of bare magnetite (**A**,**C**) and magnetite/gold NPs (**B**,**D**).
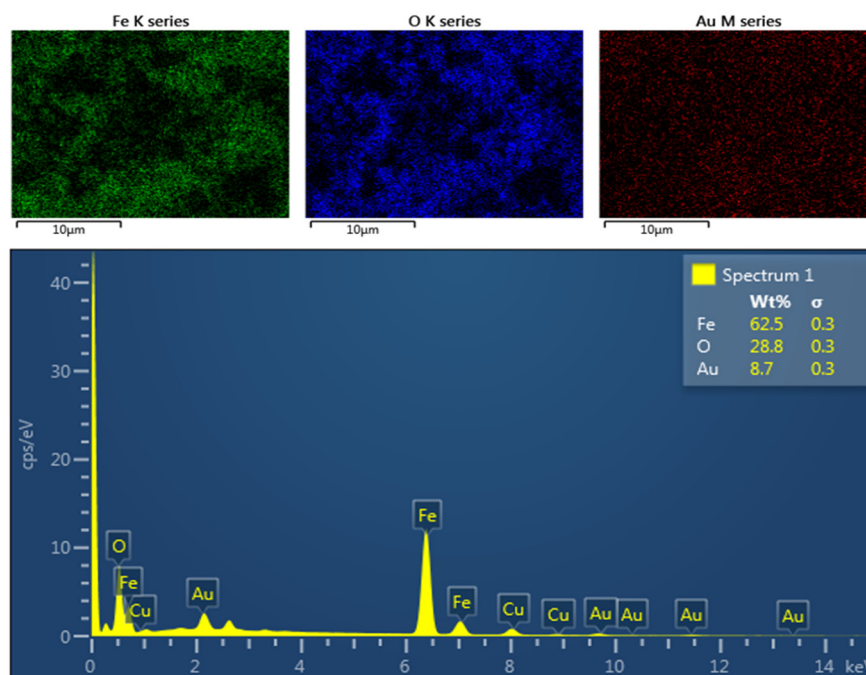
Figure 5. EDS mapping and EDS spectra of magnetite/gold NPs.

UV-Visible spectroscopy was performed to ascertain the presence of the surface plasmon resonance (SPR) band in the synthesized magnetite/gold NPs. The UV-Visible spectra of magnetite/gold NPs were compared to that of bare magnetite and bare AuNPs, summarized in Figure 6. An absorption peak was not observed for magnetite NPs in the visible range. The characteristic SPR of bare AuNPs was observed at 520 nm, consistent with AuNPs exhibiting a mean size diameter of 10–15 nm (for further details on bare AuNPs, see Appendix C). An SPR band was also present in the magnetite/gold NPs, with a bathochromic shift from 520 to 530 nm and a broadening of the absorption band, which can be attributed to the interaction between the core and shell interfaces and changes in the NPs surface [22,48,49]. Bathochromic shifts are related to changes in the dielectric constant and interaction among nanoparticles, which can be ascribed to quantum-size effects and a higher electronic density provided by the gold coating in the modified nanostructures. This is consistent with a magnetite/gold interface rather than a magnetite-gold composite [39,49].
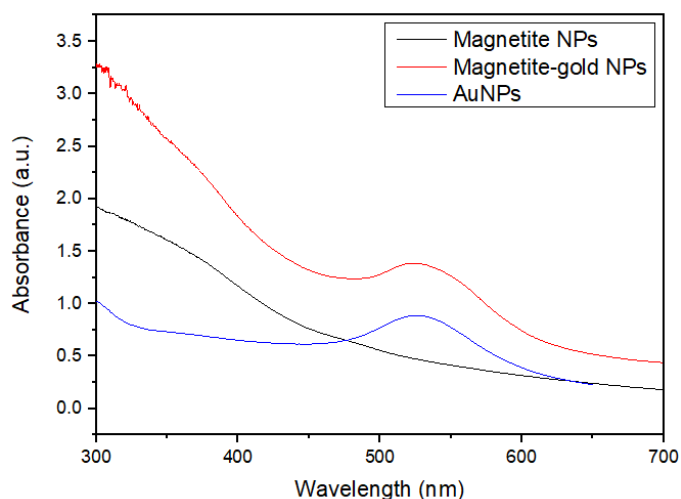

Figure 6. UV-Visible spectra of bare magnetite, bare AuNPs, and magnetite/gold NPs.

Bare magnetite and magnetite/gold NPs were characterized through DLS measurements, which indicated an average D_h of 28 ± 7 nm for bare MNPs, and 35 ± 9 nm for magnetite/gold NPs, as summarized in Table 1. The values obtained are higher than those observed from TEM measurements, as DLS provides information regarding the solvation sphere or the stabilizing agents surrounding the NPs. Magnetite and magnetite/gold NPs have negative ζ-potential values due to the contribution of TMAH on the surface of the magnetite core [22,47]. The changes in the ζ-potential value upon coating could be attributed to the thin Au layer. Finally, the PDI values below 0.7 indicate that the developed NPs present monodispersity [48] and are not prone to rapid agglomeration or precipitation, supported by the observed ζ-potential values in the ±10–30 mV range [50,51].

Table 1. Hydrodynamic diameter (D_h), ζ-potentials, and PDI of bare magnetite and magnetite/gold NPs.

Sample	D_h (nm)	ζ-Potential (mV)	PDI
Magnetite NPs	28 ± 7	-43 ± 5	0.21
Magnetite/gold NPs	35 ± 9	-19 ± 7	0.58

3.2. Characterization of the Synthesized βCDNSs-Magnetite/Gold System

The FE-SEM and EDS characterization techniques analyzed the morphology and the deposition of magnetite/gold NPs onto the as-synthesized βCDNSs. Figure 7A exposes the rough surface of βCDNSs, consistent with the structure previously reported for βCD polymers synthesized with DPC as cross-linking agent [29,52–54]. Characterization employing EDS mapping analysis evidenced the presence of C, O, and Fe in the organic substrate and the uniform distribution of magnetite/gold NPs all over the βCDNSs (Figure 7B–D, respectively). The localization of Au, using EDS mapping (Figure 7E), provides evidence that the core-shell interface is preserved upon immobilization onto the organic polymer, suggesting that most of the magnetite NPs were coated with gold. The EDS spectra of the βCDNSs-magnetite/gold system revealed its elemental composition and the presence of O, Fe, and Au (Figure 7F).
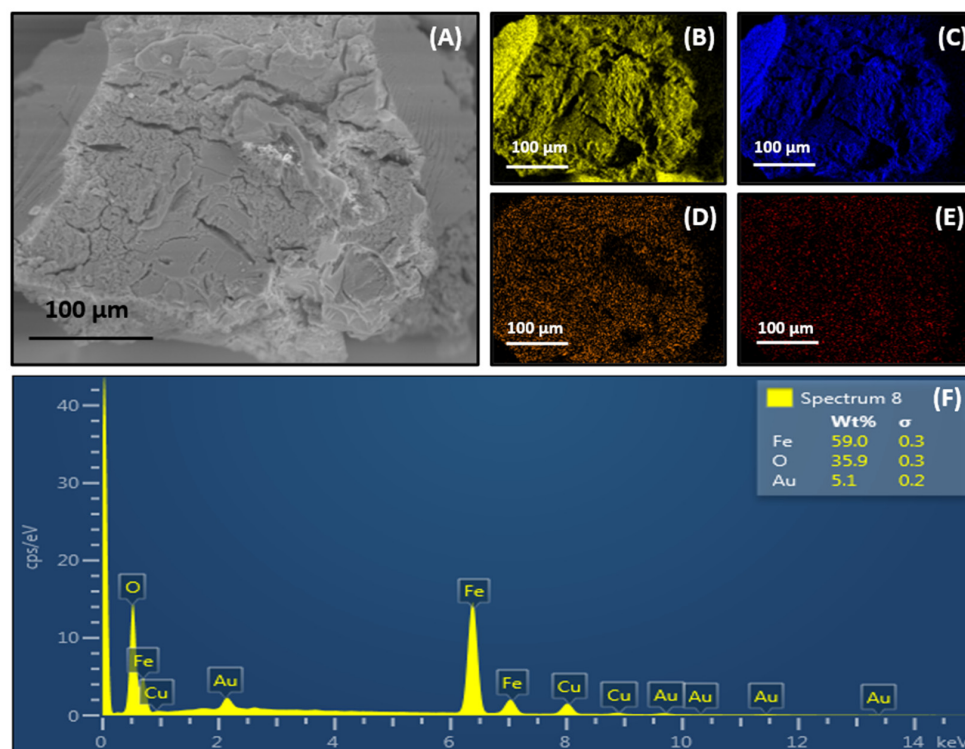

Figure 7. FE-SEM (**A**), EDS mapping, confirming the presence of carbon (**B**), oxygen (**C**), iron (**D**), and gold (**E**), EDS spectra (**F**) of the magnetite/gold NPs associated with βCDNSs.

In addition, TEM analysis was performed to ascertain the morphology and integrity of magnetite/gold NPs upon association with βCDNSs. The micrographs are illustrated in Figure 8. Magnetite/gold NPs retain their mean size (~20 nm, see Appendix B, Figure A2) and spherical morphology after deposition onto the polymer. However, it is possible to observe both dispersion and aggregation of the core-shell NPs (Figure 8A). The SAED pattern displayed in Figure 8A proved the crystalline structure of the NPs, and the identified planes are consistent with those observed in Figure 4B. Moreover, Figure 8B emphasizes that the core NPs correspond to magnetite NPs and that the thin layer corresponds to an Au shell, as supported by the crystalline planes provided by HR-TEM.
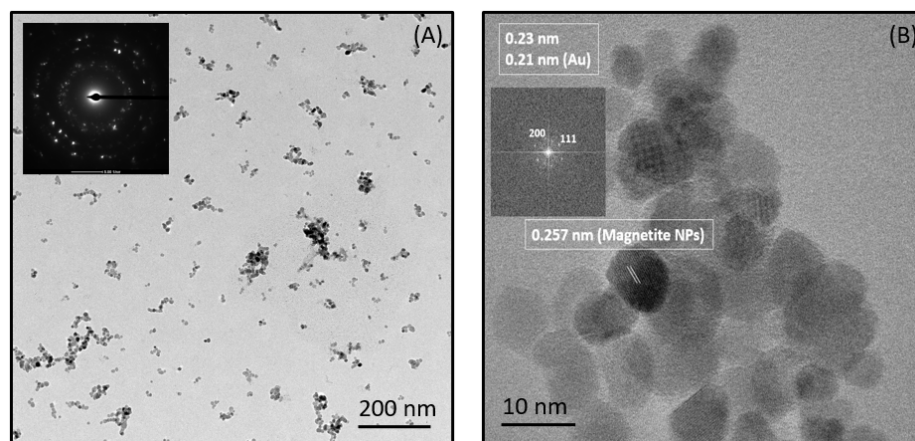

Figure 8. TEM and SAED of the magnetite/gold NPs deposited on the βCDNSs substrate (**A**), lattice fringes of magnetite and gold in the βCDNSs-magnetite/gold NPs system observed with HR-TEM (**B**).

The magnetization saturation of the βCDNSs-magnetite/gold system was evaluated to determine if the magnetite/gold NP's superparamagnetic nature is preserved upon association with the cyclodextrin polymer. Figure 9 depicts the hysteresis curves of magnetite/gold NPs and the βCDNSs-magnetite/gold system. VSM analysis shows that both systems present superparamagnetic behavior, with coercivity and remanence values near zero. However, the comparison of the curves demonstrated that the magnetization saturation drastically decreased concerning bare magnetite/gold NPs (78.3 emu/g) upon immobilization into the βCDNSs polymer (17.7 emu/g) due to the diamagnetic nature of the latter [43,52].
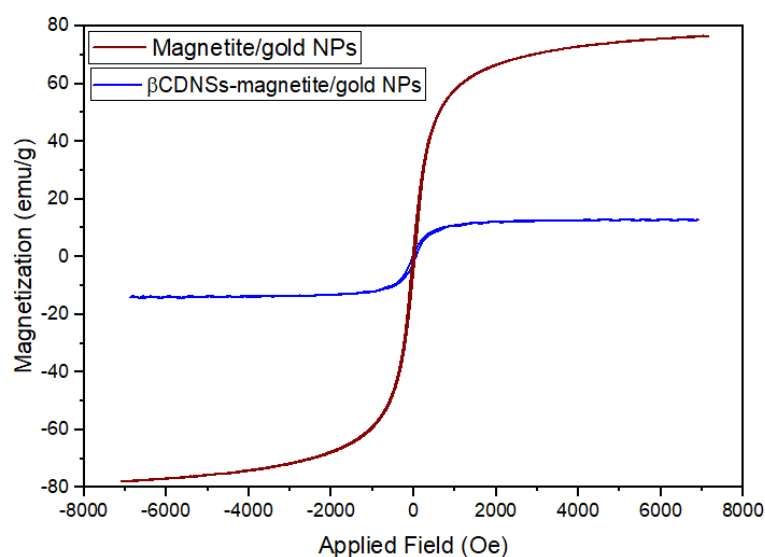

Figure 9. VSM of magnetite/gold NPs and the βCDNSs-magnetite/gold system.

Furthermore, the shielding effect due to the presence of diamagnetic gold on the surface of the magnetite core also contributes to the decrease in the saturation magnetization value and the interruption of the long-range order magnetic exchange interaction coupling upon coating with gold atoms [55,56]. Nonetheless, the developed systems present low coercivity and remanence, making them suitable candidates for biological, medical, and controlled drug release applications.

UV-Visible spectroscopy was performed to elucidate the presence of the SPR band in the βCDNSs-magnetite/gold system. The maximum absorption band in βCDNSs-magnetite/gold NPs was observed at 560 nm, evidence of a bathochromic shift from the 530 nm absorption band in the magnetite/gold NPs (see Figure 10). The red-shifted displacement of the SPR band could be attributed to the changes in the magnetite/gold NPs' chemical environment and their dielectric constant. The deposition of the NPs onto the βCDNSs matrix, dispersed and aggregated in the organic substrate, as observed in the TEM micrographs (Figure 8A), might also promote a broadening and shifting of the SPR [30,57].
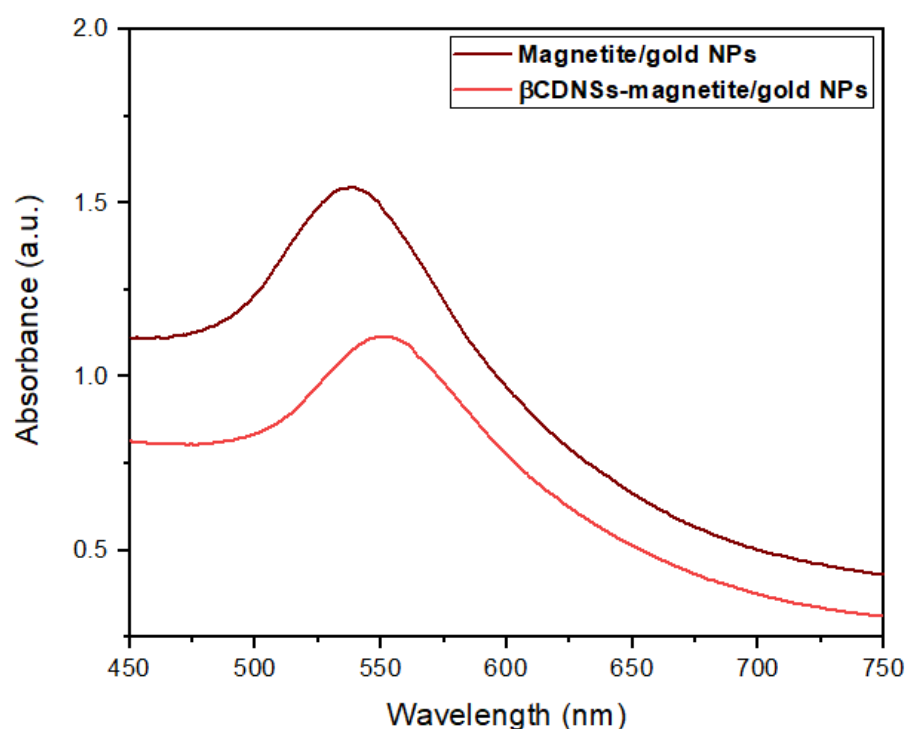

Figure 10. UV-Visible spectra of magnetite/gold NPs and the βCDNSs-magnetite/gold system.

FT-IR spectra of βCDNSs and βCDNSs-magnetite/gold NPs were determined to ascertain the interactions of the core-shell system with the polymer, as shown in Figure 11. FT-IR spectra of bare βCDNSs evidenced vibrational bands of 1039 cm^{-1} (C-O-C, stretching), 1100 cm^{-1} (OH, bending), 1477 cm^{-1} (C-H, bending), 2728 cm^{-1} (C-H, stretching), 3158 cm^{-1} (OH, stretching), and 1625 cm^{-1} (C=O, stretching). The observed vibrational spectra indicated that the βCDNSs bands are consistent with that of a cross-linked βCD [33,40]. Moreover, the FT-IR spectra of βCDNSs associated with magnetite-gold NPs displayed the characteristic peaks of the polymer, but with shifts in their location and intensity, due to the changes in the chemical environment of the functional groups and their interaction with magnetite-gold NPs. The shift of the C=O stretching peak of βCDNSs allowed us to infer that the carbonyl group is coordinated with the magnetite-gold NPs. Moreover, the FT-IR spectra of βCDNSs-magnetite/gold NPs showed 578 and 628 cm^{-1} stretching frequencies, attributed to the core-shell system's Fe-O bond [58,59].
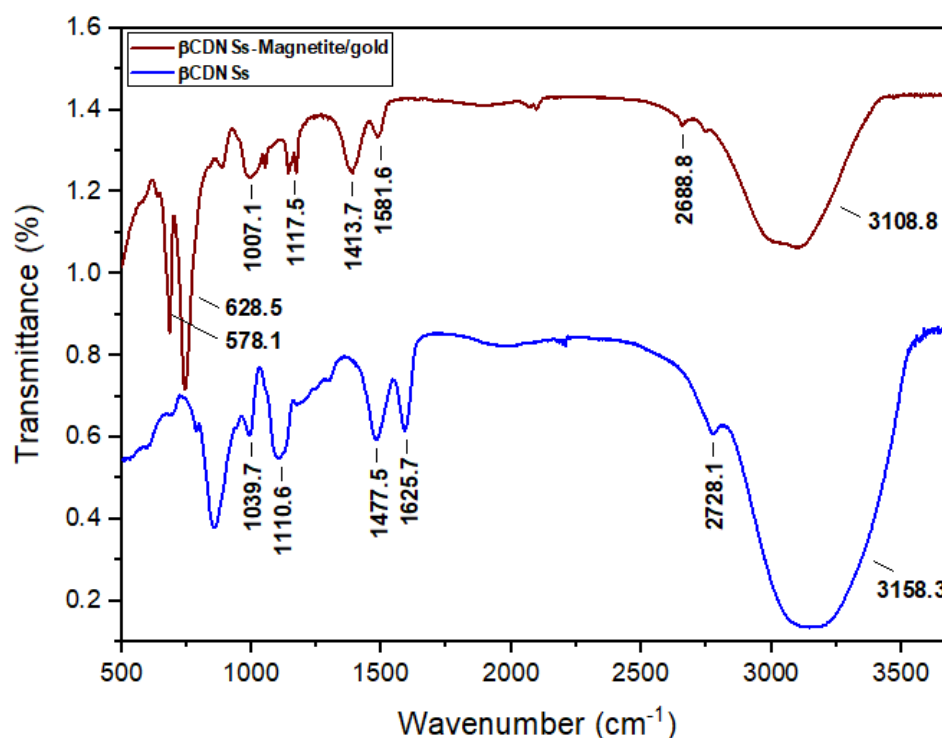
Figure 11. FT-IR spectra of βCDNSs and βCDNSs-magnetite/gold NPs.

The utility of βCDNSs as a substrate to prevent agglomeration of the magnetite/gold NPs was studied through DLS and ζ-potential measurements. As described by Table 2, bare βCDNSs present D_h within the nanometric range (>200 nm). In contrast, the PDI and ζ-potential values indicate the colloidal stability (±31 mV) and monodispersity (PDI > 0.7) of the polymer. The resistance to aggregation, nanometric dimensions, and monodispersity is retained after its modification with magnetite/gold NPs, which is relevant for potential in vivo or drug encapsulation applications [7,60,61]. Furthermore, the PDI and ζ-potential values of βCDNSs-magnetite/gold demonstrate that the colloidal stability of the core-shell NPs is improved after their deposition in the cross-linked cyclodextrins (for further information on the stability of all systems, see Appendix D).

Table 2. Hydrodynamic diameter (D_h), ζ-potentials, and PDI of βCD-NSs and βCDNSs-magnetite-AuNPs.

Sample	D_h (nm)	ζ-Potential (mV)	PDI
βCDNSs	168 ± 11	-31 ± 7	0.33
βCDNSs-Magnetite/gold	177 ± 17	-22 ± 5	0.41

AAS was performed to determine the Fe and Au content in the magnetite/gold and βCDNSs-magnetite/gold formulations for potential biomedical and drug release applications. The quantitative analysis is summarized in Table 3, which showed a Fe content of 163 and 83 mg/L in the magnetite/gold and βCDNSs-magnetite/gold NPs, respectively. Au content was 23 mg/L for the magnetite/gold core-shell structure and 11 mg/L for the βCDNSs-magnetite/gold NPs. Furthermore, a Fe/Au ratio of 7.1 for the magnetite/gold NPs was estimated, which is retained upon immobilization onto the organic βCDNSs substrate. Together, these results confirm that βCDNSs provide stability to the core-shell nanoparticles and contribute to retaining their integrity and magneto-plasmonic properties.

Table 3. Fe and Au content in the magnetite/gold and βCDNSs-magnetite/gold formulations.

Sample	Fe (mg/L)	Au (mg/L)	Fe/Au Ratio
Magnetite/gold NPs	163.3 ± 2.8	22.7 ± 3.1	7.1
βCDNSs-Magnetite/gold	83.5 ± 3.3	10.5 ± 1.7	7.9

4. Conclusions

Magnetite/gold core-shell NPs were synthesized with a narrow size distribution, assisted by adding TMAH as a surfactant. Magnetite NPs with a thin Au layer were obtained, confirming the formation of a core-shell interface through HR-TEM, FE-SEM, DLS, ζ-potential, EDS, SAED, VSM, and UV-Visible analyses while also providing valuable information on the superparamagnetic and plasmonic behavior in the nanohybrid structure. Further, the magnetite/gold NPs were associated with βCDNSs to obtain a magneto-plasmonic polymer. Characterization using SEM, EDS, FT-IR, VSM, DLS, ζ-potential, UV-Visible, AAS, and HR-TEM confirms that the βCDNSs provide a proper environment for the stabilization of the magnetite/gold NPs without compromising their magneto-plasmonic integrity while retaining the rough surface of the cyclodextrin polymer. The only drawback could be the decrease in the magnetization saturation of magnetite/gold NPs upon association due to the diamagnetic nature of the cyclodextrin polymer. Nevertheless, the developed βCDNSs-magnetite/gold system presents a novel and unique material with prospects in pharmaceutical formulations, cell viability assays, drug encapsulation, and controlled drug delivery.

Appendix A

Figure A1. Magnetic response (neodymium magnet, 5000 G) of the synthesized magnetite-Au core shell NPs.
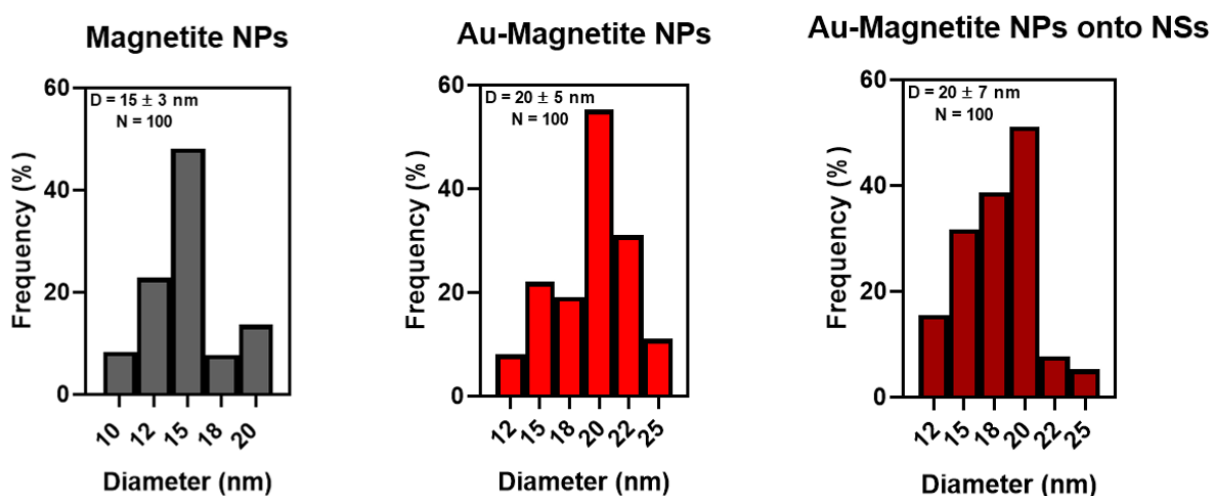
Appendix B

Figure A2. Distribution sizes of bare magnetite, Au-magnetite, and magnetite/gold NPs associated with βCDNSs measured from TEM micrographs.

Appendix C. Synthesis and Characterization of AuNPs

Bare AuNPs were synthesized and characterized using the Turkevich method for comparison purposes [62]. Briefly, 100 mL of a $HAuCl_4$ solution (1 mM) was added to a 200 mL flask with three necks equipped with a condenser. Further, the aqueous solution of $HAuCl_4$ was refluxed under stirring conditions. Then, 10 mL of sodium citrate (38.8 mM) solution was heated at 60 °C for 5 min and quickly added to the $HAuCl_4$ solution. The reflux was kept for 30 min until a red solution appeared. The obtained AuNPs were allowed to cool at room temperature, filtered using a 0.45 µm cellulose acetate membrane, and set to pH 8.8 using a 1 M NaOH solution.

To ascertain its differences from the synthesized magnetite-Au core-shell NPs, the obtained AuNPs were characterized using TEM and UV-Visible spectroscopy, as illustrated in Figure A3.
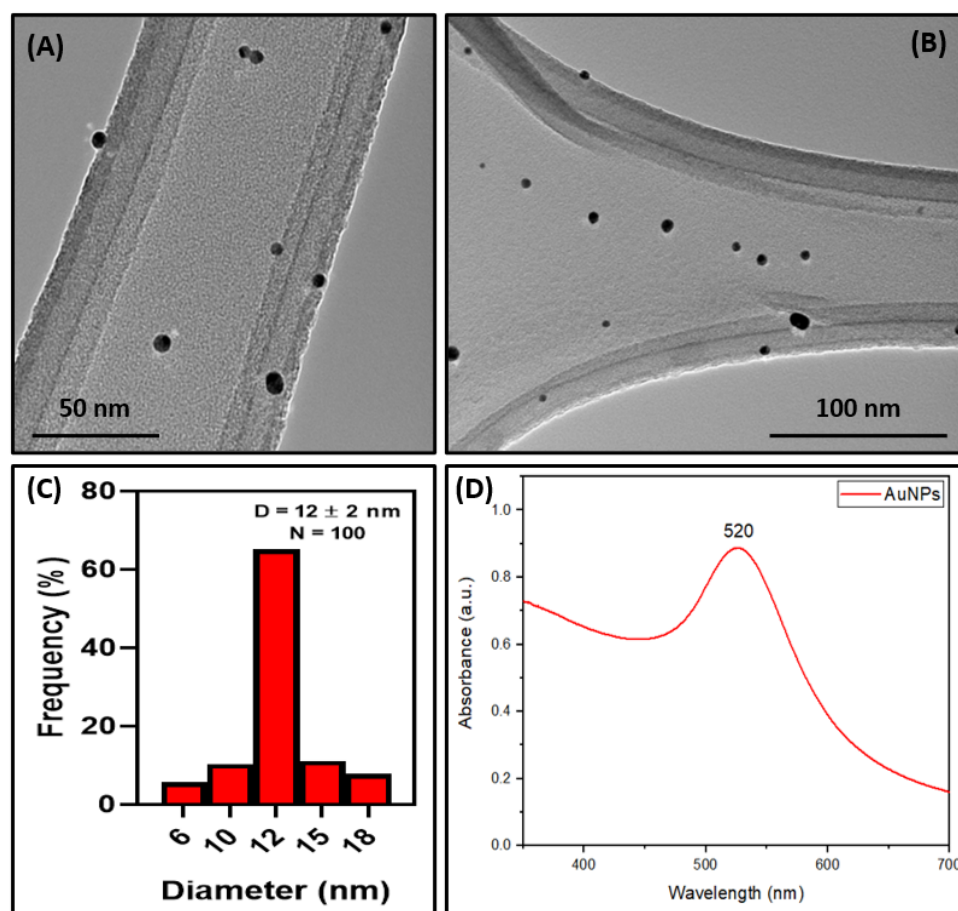
Figure A3. TEM micrographs (**A**,**B**), distribution size (**C**), and UV-Visible spectra (**D**) of bare AuNPs used as control.

Appendix D. Colloidal Stability of Magnetite-Au NPs, βCDNSs, and βCDNSs-Magnetite-Au NPs after Ten Days of Storage at Room Temperature

The hydrodynamic diameters, colloidal stability, and PDI of magnetite-Au NPs, βCDNSs, and βCDNSs-magnetite-Au NPs were evaluated at room temperature after ten days of storage. The magnetite-Au NPs displayed slight changes, evidencing an increase in the D_h, which might be ascribed to the agglomeration of the core-shell system. This is supported by a decrease in the ζ-potential values and an increase in PDI. Notably, the D_h, ζ-potential, and PDI of βCDNSs-magnetite-Au NPs showed no significant changes upon ten days, confirming the system's stability, as depicted in Table A1.

Table A1. Hydrodynamic diameter (D_h), ζ-potentials, and PDI of magnetite-Au NPs, βCD-NSs, and βCDNSs-magnetite-AuNPs after ten days of storage at room temperature.

Sample	D_h (nm)	ζ-Potential (mV)	PDI
βCDNSs	170 ± 13	-30 ± 8	0.35
Magnetite/gold NPs	41 ± 11	-13 ± 5	0.63
βCDNSs-Magnetite/gold	181 ± 20	-21 ± 7	0.44

References

1. Sood, A.; Arora, V.; Shah, J.; Kotnala, R.K.; Jain, T.K. Ascorbic acid-mediated synthesis and characterisation of iron oxide/gold core–shell nanoparticles. *J. Exp. Nanosci.* **2016**, *11*, 370–382. [CrossRef]
2. Salihov, S.V.; Ivanenkov, Y.A.; Krechetov, S.P.; Veselov, M.S.; Sviridenkova, N.V.; Savchenko, A.G.; Klyachko, N.L.; Golovin, Y.I.; Chufarova, N.V.; Beloglazkina, E.K.; et al. Recent advances in the synthesis of Fe$_3$O$_4$@AU core/shell nanoparticles. *J. Magn. Magn. Mater.* **2015**, *394*, 173–178. [CrossRef]

3. León-Félix, L.; Chaker, J.; Parise, M.; Coaquira, J.A.H.; De Los Santos Valladares, L.; Bustamante, A.; Garg, V.K.; Oliveira, A.C.; Morais, P.C. Synthesis and characterization of uncoated and gold-coated magnetite nanoparticles. *Hyperfine Interact.* **2014**, *224*, 179–188. [CrossRef]

4. Robinson, I.; Tung, L.D.; Maenosono, S.; Wälti, C.; Thanh, N.T.K. Synthesis of core-shell gold coated magnetic nanoparticles and their interaction with thiolated DNA. *Nanoscale* **2010**, *2*, 2624–2630. [CrossRef] [PubMed]

5. Izadiyan, Z.; Shameli, K.; Miyake, M.; Teow, S.Y.; Peh, S.C.; Mohamad, S.E.; Mohd Taib, S.H. Green fabrication of biologically active magnetic core-shell Fe_3O_4/Au nanoparticles and their potential anticancer effect. *Mater. Sci. Eng. C* **2019**, *96*, 51–57. [CrossRef]

6. Mohammed, L.; Gomaa, H.G.; Ragab, D.; Zhu, J. Magnetic nanoparticles for environmental and biomedical applications: A review. *Particuology* **2017**, *30*, 1–14. [CrossRef]

7. Ganapathe, L.S.; Mohamed, M.A.; Yunus, R.M.; Berhanuddin, D.D. Magnetite (Fe_3O_4) nanoparticles in biomedical application: From synthesis to surface functionalisation. *Magnetochemistry* **2020**, *6*, 68. [CrossRef]

8. Anik, M.I.; Mahmud, N.; Al Masud, A.; Hasan, M. Gold nanoparticles (GNPs) in biomedical and clinical applications: A review. *Nano Sel.* **2022**, *3*, 792–828. [CrossRef]

9. Jara-Guajardo, P.; Cabrera, P.; Celis, F.; Soler, M.; Berlanga, I.; Parra-Muñoz, N.; Acosta, G.; Albericio, F.; Guzman, F.; Campos, M.; et al. Gold nanoparticles mediate improved detection of β-amyloid aggregates by fluorescence. *Nanomaterials* **2020**, *10*, 690. [CrossRef]

10. Gao, Q.; Zhang, J.; Gao, J.; Zhang, Z.; Zhu, H.; Wang, D. Gold Nanoparticles in Cancer Theranostics. *Front. Bioeng. Biotechnol.* **2021**, *9*, 647905. [CrossRef]

11. Espinosa, A.; Bugnet, M.; Radtke, G.; Neveu, S.; Botton, G.A.; Wilhelm, C.; Abou-Hassan, A. Can magneto-plasmonic nanohybrids efficiently combine photothermia with magnetic hyperthermia? *Nanoscale* **2015**, *7*, 18872–18877. [CrossRef]

12. Bolaños, K.; Celis, F.; Garrido, C.; Campos, M.; Guzmán, F.; Kogan, M.J.; Araya, E. Adsorption of bovine serum albumin on gold nanoprisms: Interaction and effect of NIR irradiation on protein corona. *J. Mater. Chem. B* **2020**, *8*, 8644–8657. [CrossRef] [PubMed]

13. Cruz, M.M.; Ferreira, L.P.; Alves, A.F.; Mendo, S.G.; Ferreira, P.; Godinho, M.; Carvalho, M.D. *Nanoparticles for Magnetic Hyperthermia*; Elsevier Inc.: Amsterdam, The Netherlands, 2017. [CrossRef]

14. Karimzadeh, I.; Aghazadeh, M.; Ganjali, M.R.; Doroudi, T.; Kolivand, P.H. Preparation and characterization of iron oxide (Fe_3O_4) nanoparticles coated with polyvinylpyrrolidone/polyethylenimine through a facile one-pot deposition route. *J. Magn. Magn. Mater.* **2017**, *433*, 148–154. [CrossRef]

15. Mills, A.M.; Strzalka, J.; Bernat, A.; Rao, Q.; Hallinan, D.T. Magnetic-Core/Gold-Shell Nanoparticles for the Detection of Hydrophobic Chemical Contaminants. *Nanomaterials* **2022**, *12*, 1253. [CrossRef]

16. Caro, C.; Gámez, F.; Quaresma, P.; Páez-Muñoz, J.M.; Domínguez, A.; Pearson, J.R.; Pernía Leal, M.; Beltrán, A.M.; Fernandez-Afonso, Y.; De La Fuente, J.M.; et al. Fe_3O_4-Au core-shell nanoparticles as a multimodal platform for in vivo imaging and focused photothermal therapy. *Pharmaceutics* **2021**, *13*, 416. [CrossRef] [PubMed]

17. Dizaji, A.N.; Yilmaz, M.; Piskin, E. Silver or gold deposition onto magnetite nanoparticles by using plant extracts as reducing and stabilizing agents. *Artif. Cells Nanomed. Biotechnol.* **2016**, *44*, 1109–1115. [CrossRef]

18. Mostaghim, S.; Naderi, M.; Ghazitabar, A. Synthesis of magnetite-gold nanoshells by means of the secondary gold resource. *J. Iran. Chem. Soc.* **2015**, *12*, 1709–1716. [CrossRef]

19. Sun, X.; Sun, S. Preparation of magnetic nanoparticles for biomedical applications. *Methods Mol. Biol.* **2017**, *1570*, 73–89. [CrossRef]

20. Nguyen, T.T.; Mammeri, F.; Ammar, S. Iron oxide and gold based magneto-plasmonic nanostructures for medical applications: A review. *Nanomaterials* **2018**, *8*, 149. [CrossRef]

21. Sokolov, A.E.; Ivanova, O.S.; Fedorov, A.S.; Kovaleva, E.A.; Vysotin, M.A.; Lin, C.R.; Ovchinnikov, S.G. Why the Magnetite–Gold Core–Shell Nanoparticles Are Not Quite Good and How to Improve Them. *Phys. Solid State* **2021**, *63*, 1536–1540. [CrossRef]

22. Smith, M.; McKeague, M.; DeRosa, M.C. Synthesis, transfer, and characterization of core-shell gold-coated magnetic nanoparticles. *MethodsX* **2019**, *6*, 333–354. [CrossRef]

23. Poulson, B.G.; Alsulami, Q.A.; Sharfalddin, A.; El Agammy, E.F.; Mouffouk, F.; Emwas, A.-H.; Jaremko, L.; Jaremko, M. Cyclodextrins: Structural, Chemical, and Physical Properties, and Applications. *Polysaccharides* **2021**, *3*, 1–31. [CrossRef]

24. Rao, B.N.; Reddy, K.R.; Fathima, S.R.; Preethi, P. Design, development and evaluation of diltiazem hydrochloride loaded nanosponges for oral delivery. *Int. J. Curr. Pharm. Res.* **2020**, *12*, 116–122. [CrossRef]

25. Hoti, G.; Caldera, F.; Cecone, C.; Pedrazzo, A.R.; Anceschi, A.; Appleton, S.L.; Monfared, Y.K.; Trotta, F. Effect of the Cross-Linking Density on the Swelling and Rheological Behavior of Ester-Bridged β-Cyclodextrin Nanosponges. *Materials* **2021**, *14*, 478. [CrossRef] [PubMed]

26. Adeoye, O.; Bártolo, I.; Conceição, J.; da Silva, A.B.; Duarte, N.; Francisco, A.P.; Taveira, N.; Cabral-Marques, H. Pyromellitic dianhydride crosslinked soluble cyclodextrin polymers: Synthesis, lopinavir release from sub-micron sized particles and anti-HIV-1 activity. *Int. J. Pharm.* **2020**, *583*, 119356. [CrossRef] [PubMed]

27. Real, D.A.; Bolaños, K.; Priotti, J.; Yutronic, N.; Kogan, M.J.; Sierpe, R.; Donoso-González, O. Cyclodextrin-modified nanomaterials for drug delivery: Classification and advances in controlled release and bioavailability. *Pharmaceutics* **2021**, *13*, 2131. [CrossRef]

28. Trotta, F.; Caldera, F.; Cavalli, R.; Soster, M.; Riedo, C.; Biasizzo, M.; Uccello Barretta, G.; Balzano, F.; Brunella, V. Molecularly imprinted cyclodextrin nanosponges for the controlled delivery of L-DOPA: Perspectives for the treatment of Parkinson's disease. *Expert Opin. Drug Deliv.* **2016**, *13*, 1671–1680. [CrossRef]

29. Mashaqbeh, H.; Obaidat, R.; Al-Shar'i, N. Evaluation and characterization of curcumin-β-cyclodextrin and cyclodextrin-based nanosponge inclusion complexation. *Polymers* **2021**, *13*, 4073. [CrossRef]

30. Salazar, S.; Yutronic, N.; Kogan, M.J.; Jara, P. Cyclodextrin nanosponges inclusion compounds associated with gold nanoparticles for potential application in the photothermal release of melphalan and cytoxan. *Int. J. Mol. Sci.* **2021**, *22*, 6446. [CrossRef]

31. Silva, N.; Muñoz, C.; Diaz-Marcos, J.; Samitier, J.; Yutronic, N.; Kogan, M.J.; Jara, P. In Situ Visualization of the Local Photothermal Effect Produced on α-Cyclodextrin Inclusion Compound Associated with Gold Nanoparticles. *Nanoscale Res. Lett.* **2016**, *11*, 1–8. [CrossRef]

32. De Vries, W.C.; Niehues, M.; Wissing, M.; Würthwein, T.; Mäsing, F.; Fallnich, C.; Studer, A.; Ravoo, B.J. Photochemical preparation of gold nanoparticle decorated cyclodextrin vesicles with tailored plasmonic properties. *Nanoscale* **2019**, *11*, 9384–9391. [CrossRef] [PubMed]

33. Salazar Sandoval, S.; Cortés-Adasme, E.; Gallardo-Toledo, E.; Araya, I.; Celis, F.; Yutronic, N.; Jara, P.; Kogan, M.J. β-Cyclodextrin-Based Nanosponges Inclusion Compounds Associated with Gold Nanorods for Potential NIR-II Drug Delivery. *Pharmaceutics* **2022**, *14*, 2206. [CrossRef] [PubMed]

34. Vellaichamy, B.; Periakaruppan, P. Silver nanoparticle-embedded RGO-nanosponge for superior catalytic activity towards 4-nitrophenol reduction. *RSC Adv.* **2016**, *6*, 88837–88845. [CrossRef]

35. Russo, M.; Spinella, A.; Di Vincenzo, A.; Lazzara, G.; Correro, M.R.; Shahgaldian, P.; Lo Meo, P.; Caponetti, E. Synergistic Activity of Silver Nanoparticles and Polyaminocyclodextrins in Nanosponge Architectures. *ChemistrySelect* **2019**, *4*, 873–879. [CrossRef]

36. Salazar Sandoval, S.; Bruna, T.; Maldonado-Bravo, F.; Bolaños, K.; Adasme-Reyes, S.; Riveros, A.; Caro, N.; Yutronic, N.; Silva, N.; Kogan, M.J.; et al. β-Cyclodextrin Nanosponges Inclusion Compounds Associated with Silver Nanoparticles to Increase the Antimicrobial Activity of Quercetin. *Materials* **2023**, *16*, 3538. [CrossRef] [PubMed]

37. Rajan, A.; Sharma, M.; Sahu, N.K. Assessing magnetic and inductive thermal properties of various surfactants functionalised Fe₃O₄ nanoparticles for hyperthermia. *Sci. Rep.* **2020**, *10*, 15045. [CrossRef]

38. Bustamante-Torres, M.; Romero-Fierro, D.; Estrella-Nuñez, J.; Arcentales-Vera, B.; Chichande-Proaño, E.; Bucio, E. Polymeric Composite of Magnetite Iron Oxide Nanoparticles and Their Application in Biomedicine: A Review. *Polymers* **2022**, *14*, 752. [CrossRef]

39. Lin, C.W.; Chen, J.M.; Lin, Y.J.; Chao, L.W.; Wei, S.Y.; Wu, C.H.; Jeng, C.C.; Wang, L.M.; Chen, K.L. Magneto-Optical Characteristics of Streptavidin-Coated Fe₃O₄@Au Core-Shell Nanoparticles for Potential Applications on Biomedical Assays. *Sci. Rep.* **2019**, *9*, 16466. [CrossRef] [PubMed]

40. Kumar, S.; Pooja; Trotta, F.; Rao, R. Encapsulation of babchi oil in cyclodextrin-based nanosponges: Physicochemical characterization, photodegradation, and in vitro cytotoxicity studies. *Pharmaceutics* **2018**, *10*, 169. [CrossRef]

41. Tanasa, E.; Zaharia, C.; Radu, I.C.; Surdu, V.A.; Vasile, B.S.; Damian, C.M.; Andronescu, E. Novel nanocomposites based on functionalized magnetic nanoparticles and polyacrylamide: Preparation and complex characterization. *Nanomaterials* **2019**, *9*, 1384. [CrossRef]

42. Andrade, Â.L.; Fabris, J.D.; Ardisson, J.D.; Valente, M.A.; Ferreira, J.M.F. Effect of Tetramethylammonium Hydroxide on Nucleation, Surface Modification and Growth of Magnetic Nanoparticles. *J. Nanomater.* **2012**, *2012*, 10. [CrossRef]

43. Montazeri, H.; Amani, A.; Shahverdi, H.R.; Haratifar, E.A.D.; Shahverdi, A.R. Separation of the defect-free Fe₃O₄-Au core/shell fraction from magnetite-gold composite nanoparticles by an acid wash treatment. *J. Nanostructure Chem.* **2013**, *3*, 2–7. [CrossRef]

44. Ijaz, I.; Gilani, E.; Nazir, A.; Bukhari, A. Detail review on chemical, physical and green synthesis, classification, characterizations and applications of nanoparticles. *Green Chem. Lett. Rev.* **2020**, *13*, 59–81. [CrossRef]

45. Ángeles-Pascual, A.; Piñón-Hernández, J.R.; Estevez-González, M.; Pal, U.; Velumani, S.; Pérez, R.; Esparza, R. Structure, magnetic and cytotoxic behaviour of solvothermally grown Fe₃O₄@Au core-shell nanoparticles. *Mater. Charact.* **2018**, *142*, 237–244. [CrossRef]

46. Salazar, S.; Guerra, D.; Yutronic, N.; Jara, P. Removal of aromatic chlorinated pesticides from aqueous solution using β-cyclodextrin polymers decorated with Fe₃O₄ nanoparticles. *Polymers* **2018**, *10*, 1038. [CrossRef] [PubMed]

47. Singh, H.; Du, J.; Singh, P.; Yi, T.H. Ecofriendly synthesis of silver and gold nanoparticles by Euphrasia officinalis leaf extract and its biomedical applications. *Artif. Cells Nanomed. Biotechnol.* **2018**, *46*, 1163–1170. [CrossRef] [PubMed]

48. Sodipo, B.K.; Aziz, A.A.; Mustapa, M. Facile synthesis and characteristics of gold coated superparamagnetic iron oxide nanoparticles via sonication. *Int. J. Nanoelectron. Mater.* **2015**, *8*, 1–6.

49. Chung, R.J.; Shih, H.T. Preparation of multifunctional Fe@Au core-shell nanoparticles with surface grafting as a potential treatment for magnetic hyperthermia. *Materials* **2014**, *7*, 653–661. [CrossRef]

50. Khalil, M.I. Co-precipitation in aqueous solution synthesis of magnetite nanoparticles using iron(III) salts as precursors. *Arab. J. Chem.* **2015**, *8*, 279–284. [CrossRef]

51. Danaei, M.; Dehghankhold, M.; Ataei, S.; Hasanzadeh Davarani, F.; Javanmard, R.; Dokhani, A.; Khorasani, S.; Mozafari, M.R. Impact of particle size and polydispersity index on the clinical applications of lipidic nanocarrier systems. *Pharmaceutics* **2018**, *10*, 57. [CrossRef]

52. Li, Z.; Ma, J.; Ruan, J.; Zhuang, X. Using Positively Charged Magnetic Nanoparticles to Capture Bacteria at Ultralow Concentration. *Nanoscale Res. Lett.* **2019**, *14*, 1–8. [CrossRef] [PubMed]

53. Omar, S.M.; Ibrahim, F.; Ismail, A. Formulation and evaluation of cyclodextrin-based nanosponges of griseofulvin as pediatric oral liquid dosage form for enhancing bioavailability and masking bitter taste. *Saudi Pharm. J.* **2020**, *28*, 349–361. [CrossRef] [PubMed]
54. Li, L.; Liu, H.; Li, W.; Liu, K.; Tang, T.; Liu, J.; Jiang, W. One-step synthesis of an environment-friendly cyclodextrin-based nanosponge and its applications for the removal of dyestuff from aqueous solutions. *Res. Chem. Intermed.* **2020**, *46*, 1715–1734. [CrossRef]
55. Salazar, S.; Yutronic, N.; Jara, P. Magnetic β-cyclodextrin nanosponges for potential application in the removal of the neonicotinoid dinotefuran from wastewater. *Int. J. Mol. Sci.* **2020**, *21*, 4079. [CrossRef]
56. Sood, A.; Arora, V.; Shah, J.; Kotnala, R.K.; Jain, T.K. Multifunctional gold coated iron oxide core-shell nanoparticles stabilized using thiolated sodium alginate for biomedical applications. *Mater. Sci. Eng. C* **2017**, *80*, 274–281. [CrossRef]
57. Silva, N.; Moris, S.; Díaz, M.; Yutronic, N.; Lang, E.; Chornik, B.; Kogan, M.J.; Jara, P. Evidence of the disassembly of α-cyclodextrin-octylamine inclusion compounds conjugated to gold nanoparticles via thermal and photothermal effects. *Molecules* **2016**, *21*, 1444. [CrossRef]
58. Caldera, F.; Nisticò, R.; Magnacca, G.; Matencio, A.; Khazaei Monfared, Y.; Trotta, F. Magnetic Composites of Dextrin-Based Carbonate Nanosponges and Iron Oxide Nanoparticles with Potential Application in Targeted Drug Delivery. *Nanomaterials* **2022**, *12*, 754. [CrossRef]
59. Roto, R.; Yusran, Y.; Kuncaka, A. Magnetic adsorbent of Fe_3O_4 @SiO_2 core-shell nanoparticles modified with thiol group for chloroauric ion adsorption. *Appl. Surf. Sci.* **2016**, *377*, 30–36. [CrossRef]
60. Antal, I.; Koneracka, M.; Kubovcikova, M.; Zavisova, V.; Khmara, I.; Lucanska, D.; Jelenska, L.; Vidlickova, I.; Zatovicova, M.; Pastorekova, S.; et al. D,L-lysine functionalized Fe_3O_4 nanoparticles for detection of cancer cells. *Colloids Surf. B Biointerfaces* **2018**, *163*, 236–245. [CrossRef]
61. Nedyalkova, M.; Donkova, B.; Romanova, J.; Tzvetkov, G.; Madurga, S.; Simeonov, V. Iron oxide nanoparticles–In vivo/in vitro biomedical applications and in silico studies. *Adv. Colloid Interface Sci.* **2017**, *249*, 192–212. [CrossRef]
62. Kimling, J.; Maier, M.; Okenve, B.; Kotaidis, V.; Ballot, H.; Plech, A. Turkevich method for gold nanoparticle synthesis revisited. *J. Phys. Chem. B* **2006**, *110*, 15700–15707. [CrossRef] [PubMed]